Biomech Model Mechanobiol
DOI 10.1007/s10237-014-0563-y

ORIGINAL PAPER

Numerical simulation of blood flow and pressure drop in the pulmonary arterial and venous circulation

M. Umar Qureshi · Gareth D. A. Vaughan · Christopher Sainsbury · Martin Johnson · Charles S. Peskin · Mette S. Olufsen · N. A. Hill

Received: 6 October 2013 / Accepted: 18 February 2014

Abstract A novel multiscale mathematical and computational model of the pulmonary circulation is presented and used to analyse both *arterial and venous* pressure and flow. This work is a major advance over previous studies by Olufsen et al. (Ann Biomed Eng 28:1281–1299, 2012) which only considered the arterial circulation. For the first three generations of vessels within the pulmonary circulation, geometry is specified from patient-specific measurements obtained using magnetic resonance imaging (MRI). Blood flow and pressure in the larger arteries and veins are predicted using a nonlinear, cross-sectional-area-averaged system of equations for a Newtonian fluid in an elastic tube. Inflow into the main pulmonary artery is obtained from MRI measurements, while pressure entering the left atrium from the main pulmonary vein is kept constant at the normal mean value of 2 mmHg. Each terminal vessel in the network of 'large' arteries is connected to its corresponding terminal vein via a network of vessels representing the vascular bed of smaller arteries and veins. We develop and implement an algorithm to calculate the admittance of each vascular bed, using bifurcating structured trees and recursion. The structured-tree models take into account the geometry and material properties of the 'smaller' arteries and veins of radii $\geq 50\,\mu$m. We study the effects on flow and pressure associated with three classes of pulmonary hypertension expressed via stiffening of larger and smaller vessels, and vascular rarefaction. The results of simulating these pathological conditions are in agreement with clinical observations, showing that the model has potential for assisting with diagnosis and treatment for circulatory diseases within the lung.

Keywords Pulmonary circulation · Pulmonary hypertension · Resistance arteries · Structured tree · Multiscale mathematical model

M. U. Qureshi
Department of Mathematics, International Islamic University, Sector H10, Islamabad 44000, Pakistan
e-mail: m.qureshi.2@research.gla.ac.uk

M. U. Qureshi · G. D. A. Vaughan · N. A. Hill (✉)
School of Mathematics and Statistics, University of Glasgow, Glasgow G12 8QW, UK
e-mail: Nicholas.Hill@glasgow.ac.uk

G. D. A. Vaughan
e-mail: gdavaughan@gmail.com

C. Sainsbury
School of Medicine, University of Glasgow, Glasgow G12 8QQ, UK
e-mail: Chris.Sainsbury@glasgow.ac.uk

M. Johnson
Scottish Pulmonary Vascular Unit, Golden Jubilee National Hospital, Glasgow G81 4D7, UK
e-mail: mjohnson4@nhs.net

C. S. Peskin
Courant Institute of Mathematical Sciences, New York University, 251 Mercer Street, New York, NY 10012, USA
e-mail: peskin@cims.nyu.edu

M. S. Olufsen
Department of Mathematics, North Carolina State University, Raleigh, NC 27502, USA
e-mail: msolufse@ncsu.edu

1 Introduction

The cardiovascular circulation is comprised of two separate systems, the systemic and the pulmonary circulations. The systemic circulation transports oxygenated blood from the left heart to organs and muscles in the body and back to the right heart, while the pulmonary circulation transports blood

Published online: 09 March 2014

from the right heart through the lungs and back to the left heart facilitating removal of CO_2 and re-oxygenation of the blood.

One-dimensional models of the circulation have been extensively used by many authors to study pressure and flow wave propagation in the systemic arteries, e.g. Olufsen et al. (2000), Sherwin et al. (2003), Formaggia et al. (2006), Azer and Peskin (2007), Matthys et al. (2007) and Reymond et al. (2009), in the cerebral circulation, e.g. Alastruey et al. (2007), Cousins et al. (2013) and Reymond et al. (2009), and coronary arterial trees, e.g. Huo and Kassab (2007), Reymond et al. (2009) and Bovendeerd et al. (2006), under normal physiological and pathological conditions. Moreover, they have been exploited to investigate the haemodynamics in systemic veins by only considering part of the venous system (Fullana and Zaleski 2009) and in closed-loop global systemic circulation models, with particular emphasis on the venous system (Müller and Toro 2014). These models are not only useful for understanding the nature of fluid-structure interaction and the mechanics of pulse waves in the cardiovascular system but they also make a good research and clinical tool, e.g. by providing suitable boundary conditions for detailed three-dimensional models (Vignon-Clementel et al. 2006), assessing the techniques for estimating in vivo pulse wave velocity (Alastruey 2011), and surgical planning (Taylor et al. 1999). For a more comprehensive overview of one-dimensional models and their applications, see Reymond et al. (2009) and Vosse and Stergiopulos (2011).

Most previous modelling studies based on one or three-dimensional analysis (e.g. Figueroa et al. 2006; Xiao et al. 2013; Vignon-Clementel et al. 2006), focus on the systemic arterial system, while relatively little attention has been given to the pulmonary circulation studied here. The lungs have a unique structure, consisting of complex network of arterial and venous vessels, airways and alveoli. To understand better the dynamics involved in predicting the propagation of flow and pressure in the pulmonary circulation, we outline similarities and differences between the two systems. Both systems transport the same volume of blood per unit time, but the pulmonary circulation is much smaller and operates at a much lower pressure, and the pulmonary arterial and venous walls are thinner and more compliant than the systemic vessels (Milnor 1989; Patel et al. 1960). Moreover, the pulmonary system only stores about 10 % (500 ml) of the total blood volume. This is still significant, given that the lungs only comprise 1 % of the total body weight (Thurlbeck and Churg 1995).

The mean driving pressure in the pulmonary arteries is about 10 mmHg[1] compared with 91 mmHg in the systemic arteries, and, since the volume flux is equal in both systems, the resistance in the pulmonary circulation is nine times less than that of systemic circulation, see Nichols and O'Rourke (1998) and Hall (2011). Furthermore, the pulmonary veins serve not only as channels through which oxygenated capillary blood flow is transported into the left atrium, but they also regulate fluid filtration pressure in the upstream capillary network via active vasomotion contributing significantly towards total pulmonary vascular resistance (Gao and Raj 2005). This suggests that in the pulmonary circulation the veins play an active role when regulating haemodynamics and the pressure drop continues over both arteries and veins, whereas in the systemic circulation the veins are passive and the majority of the pressure drop can be found within the arteries and arterioles. Although in both the systemic and pulmonary circulations the precapillary arterioles are the major site of resistance under both normal and hypoxic conditions (Burton 1972; Barnes and Liu 1995; Levy et al. 2001; Olufsen et al. 2012; Pries et al. 1995), there is still some confusion as to the relative contribution of arteries, capillaries and veins to total resistance to the flow in the lungs (Burton 1972; Gao and Raj 2005). Some results (Levy et al. 2001; Pries et al. 1995; Zhuang et al. 1983) suggest that the precapillary pressure drop takes place across the small vessels of diameter 10–300 μm making the vascular beds the location of maximum resistance to the blood flow and the greatest pressure drop. The only study that has attempted to use computation to assess the pressure drop over both large and small vessels is by Olufsen et al. (2012), who predicted the pressure drop across the systemic vascular beds using a structured-tree model. To our knowledge, there is no study that includes the effects of both arterioles and venules on microcirculatory characteristics of blood flow in the pulmonary circulation.

In this paper, we develop a mathematical model and numerical algorithms allowing prediction of the pressure drop and pulse wave propagation for the combined pulmonary arterial and venous system. The model includes all arteries and veins of radii >50 μm. The large arteries and veins, with radii >4.5 mm, are represented explicitly, and pulse wave propagation within these vessels is predicted by solving the 1D Navier–Stokes equation for a Newtonian fluid using a Lax–Wendroff numerical scheme. Flow and pressure in the small arteries and veins with radii between 4.5 mm and 50 μm are computed via solutions to linearised equations solved in vessel networks (vascular beds) consisting of pairs of structured trees connected at their smallest (terminal) branches. A total admittance matrix is derived for each vascular bed using a fast recurrence relation. For each vascular bed, the admittance matrix provides a boundary condition linking pressures and volume fluxes between smallest (terminal) large arteries and the corresponding large veins. The analysis is further extended to prediction of the mean pressure drop within the vascular beds. Finally, this new pulmonary model is applied to analyse three clinical conditions asso-

[1] As is common for studies of cardiovascular dynamics, all pressures are given in mmHg. The conversion to SI units is 1 mmHg = 133.3 Pa.

ciated with pulmonary hypertension, viz. pulmonary arterial hypertension (PAH) associated with increased resistance and stiffening of pulmonary arterioles and venules, vascular remodelling (HLD) associated with hypoxic lung disease and chronic thromboembolic pulmonary hypertension (CTEPH) represented by increased stiffness of the large pulmonary arteries. Results from our study show good agreement with clinical observations (Lankhaar et al. 2006).

2 Methods

The pulmonary circulation illustrated in Fig. 1 consists of large arteries and veins organised in a tree-like structure. The main pulmonary artery (MPA) emanates from the right ventricle and bifurcates into two vessels, the right (RPA) and left (LPA) pulmonary arteries transporting blood to the right and left lungs. As the heart is located on the left side of the body, the RPA is significantly longer than the LPA. These two main vessels further bifurcate into the right and left interlobular arteries (RIA and LIA) and the right and left trunk arteries (RTA and LTA). Arteries continue to bifurcate following a structured branching scheme in which daughter vessels are scaled relative to parent vessels (Weibel 2009). The branching pattern continues until the level of the bronchia where the capillaries loop around the bronchi to facilitate maximal perfusion of oxygen and carbon dioxide with the lungs. The venous vessels closely follow the branching patterns of the arteries, with the exception of the four large veins (the right and left inferior veins (RIV and LIV) and the right and left superior pulmonary veins (RSV and LSV)), which deliver blood to the left atrium. For this study, we separate arteries and veins into two groups; the large vessels, i.e. the MPA, R/LPA, R/LIA, R/LTA, R/LIV and R/LSV, which are modelled explicitly, and the small vessels, including the small arteries (arterioles) and veins (venules), which are represented by structured trees. The smallest capillaries offer little flow resistance (Fung 1996) and are therefore not included in the model. In the large vessels, nonlinear inertial effects cannot be neglected, whereas for the smaller vessels viscous effects play an important role. This separation is similar to earlier studies (Olufsen et al. 2000, 2012; Steele et al. 2007); however, none of these considered the effect of the venous circulation. One study by Li and Cheng (1993) does include both arteries and veins, but this study uses a lumped parameter model to represent the small vessels, so it is not possible to predict the pressure drop over the complete system. Moreover, since the pulmonary veins contribute towards overall vascular resistance that regulate flow in pulmonary arteries, studying the pulmonary arterial system in isolation is not adequate.

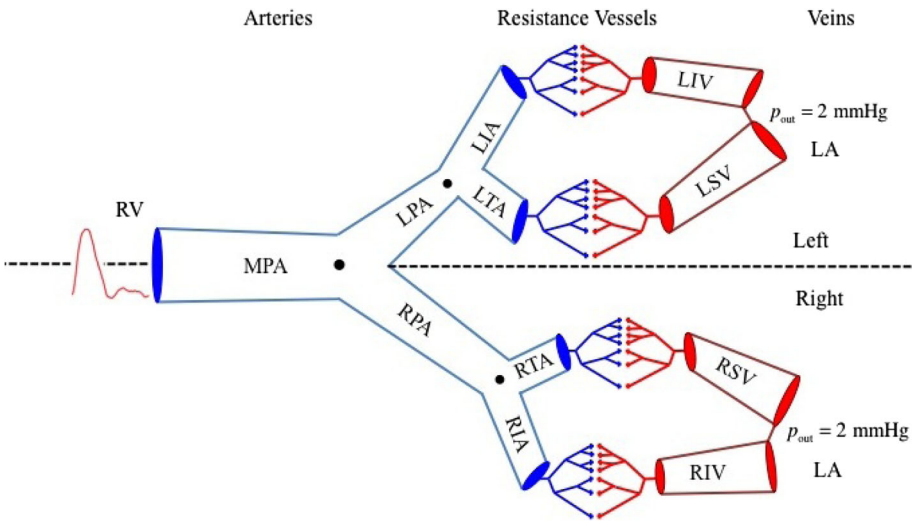

Fig. 1 Schematic of the pulmonary circulation model arranged in a sequence of larger arteries, arterioles, venules and large veins. The large pulmonary arteries and veins are specified explicitly, while the small vessels are represented by structured trees. The main pulmonary artery (MPA) is the root vessel within the pulmonary arterial tree. A flow waveform measured using MRI is specified at the inlet to this vessel. The MPA bifurcates into the right (RPA) and left (LPA) pulmonary arteries. The RPA bifurcates into the right interlobular artery (RIA) and the right trunk artery (RTA), and the LPA bifurcates into the left interlobular artery (LIA) and left trunk artery (LTA). The RIA, RTA, LIA and LTA are the *terminal* vessels of the large pulmonary arterial model, and it is to the outlet of these vessels that the structured-tree matching conditions are applied to join the arterial and venous systems. The outlet of the RIA is matched with the inlet of right inferior pulmonary vein (RIV), the RTA with the right superior vein (LSV), the LIA with the left inferior vein (LIV), and the LTA with the inlet of left superior vein (LSV). The pulmonary veins open into left atrium in pairs draining blood from left and right lungs, and therefore at the outlet of each vein, a constant pressure condition is applied. Continuous-pressure and flow-conservation conditions are used at each bifurcating junction, marked by a **'.'** for large arteries

In Olufsen et al. (2012), we adapted the 1D fluid dynamics model of Olufsen (1999) to predict blood flow and pressure in the pulmonary arteries. Here, we use a similar approach to predict flow and pressure in a complete network including pulmonary arteries and veins. An important feature of the complete pulmonary circulation model is our new methodology developed to connect arterial and venous structured trees.

2.1 The large arteries and veins

We first describe the geometry used for generating the domain for the computational model, and secondly, we discuss how the haemodynamics is computed in the large vessels.

Vessel geometry As in our previous study (Olufsen et al. 2012), the geometry of the large pulmonary arteries was specified from MRI measurements from a healthy young volunteer. Figure 1 shows a schematic of the pulmonary circulation network including the first three generations of the pulmonary arteries and the large pulmonary veins. For these vessels, lengths and diameters are summarised in Table 1. The large vessels are connected to structured trees including small arteries/arterioles and veins/venules.

It is often difficult to locate the large pulmonary veins because their geometry and orientation vary significantly even between healthy individuals, and thus, to limit the time the subject was in the MRI scanner, these vessels (numbered 8–11 in Table 1) were not measured. Consequently, we constructed a model of the most common healthy pulmonary venous geometry, in which the four left and right, superior and inferior pulmonary veins return the oxygenated blood from both lungs into the left atrium (Kato et al. 2003). The dimensions of these veins were obtained from literature (Kawahira et al. 1997; Kim et al. 2005) and adjusted to meet the requirements of the numerical scheme that the distal diameter of each terminal large artery (i.e. the RIA, RTA, LIA and LTA) must be the same as the distal diameter of its matching terminal vein (RSV, RIV, LSV and LIV, respectively) (Fig. 1).

Table 1 Dimensions of the large pulmonary vessels including the main pulmonary artery (MPA), the right (RPA) and left (LPA) pulmonary arteries, the right (RIA) and left (LIA) interlobular arteries, the right (RTA) and left (LTA) trunk arteries, the right (RSV) and left (LSV) superior veins, and the right (RIV) and left (LIV) inferior veins

No.	Name	Prox. diam. (cm)	Dist. diam. (cm)	Length (cm)
1	MPA	2.7	2.6	4.50
2	RPA	1.8	1.2	5.75
3	LPA	2.2	2.2	2.50
4	RIA	1.1	1.1	1.25
5	RTA	0.9	0.9	1.00
6	LIA	2.1	1.8	2.25
7	LTA	1.2	1.2	1.00
8	RIV	1.2	1.1	1.25
9	RSV	1.0	0.9	1.50
10	LIV	1.9	1.8	2.25
11	LSV	1.3	1.2	2.00

For each vessel, the proximal and distal diameters are given together with the vessel lengths. For both arteries and veins, proximal and distal refer to vessel entry close to and away from heart. The measurement resolution for all diameters is 1 mm, and all vessel lengths are rounded to the nearest 2.5 mm to match the spatial resolution used in numerical computations. The RTA and LTA were too short to obtain both inlet and outlet diameters; thus, these vessels were assumed not to taper and their lengths were estimated from literature

2.1.1 Large-vessel fluid dynamics

Blood flow in the large compliant pulmonary arteries and veins is computed using the approach put forward by Olufsen (1999), Olufsen et al. (2000) and Olufsen et al. (2012) in which volumetric flow rate, blood pressure, and cross-sectional area was predicted in time along one spatial dimension. These quantities are predicted using two equations ensuring conservation of volume and momentum, combined with a constitutive equation relating vessel cross-sectional area to blood pressure.

Conservation of volume is satisfied by

$$\frac{\partial q}{\partial x} + \frac{\partial A}{\partial t} = 0, \tag{1}$$

where $q(x,t)$ denotes the volumetric flow along any given vessel and $A(x,t)$ denotes the corresponding cross-sectional area. These quantities are functions of the distance x along the vessels and time t. Assuming a flat velocity profile with a thin boundary layer,

$$u = \begin{cases} \overline{u} & \text{for} \quad r \leq R - \delta \\ \overline{u}(R-r)/\delta & \text{for} \quad R - \delta < r \leq R \end{cases} \tag{2}$$

with constant central velocity $\overline{u}$, the momentum balance equation can be written as

$$\frac{\partial q}{\partial t} + \frac{\partial}{\partial x}\left(\frac{q^2}{A}\right) + \frac{A}{\rho}\frac{\partial p}{\partial x} = -\frac{2\pi\nu R}{\delta}\frac{q}{A}, \tag{3}$$

where ρ (constant) denotes the density of the fluid, $p(x,t)$ the pressure, ν (constant) the kinematic viscosity, δ (constant) the boundary layer thickness and $R(x,t)$ the vessel radius.

Finally, the constitutive equation relating pressure $p(x,t)$ and cross-sectional area $A(x,t)$ can be obtained assuming that the deformation of the wall can be modelled as a thin elastic membrane, giving

$$p(x,t) - p_0 = \frac{4}{3}\frac{Eh}{r_0}\left(1 - \sqrt{\frac{A_0}{A}}\right), \tag{4}$$

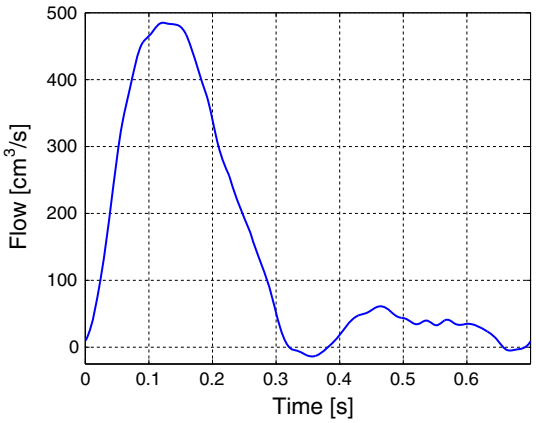

Fig. 2 Inflow profile for the main pulmonary artery. This profile was interpolated from MRI measurements sampled at 45 points per period and averaged over five cardiac cycles

where p_0 denotes the external pressure, E Young's modulus, h the vessel wall thickness and r_0 the vessel radius associated with $p(x,t) = p_0$. From these quantities, the unstressed vessel area A_0 can be computed as $A_0 = \pi r_0^2$.

The above system of equations is hyperbolic; thus, for each vessel, a boundary condition must be applied at each end. For the MPA, the flow is specified at the inlet (see Fig. 1) using the MRI measured flow rate waveform shown in Fig. 2. At each bifurcation, two conditions are needed connecting outflow from the parent vessel and inflow to the daughter vessels. These are imposed by ensuring continuity of pressure and conservation of flow, i.e.

$$p_{\mathrm{p}}(L,t) = p_{d_1}(0,t) = p_{d_2}(0,t),$$
$$q_{\mathrm{p}}(L,t) = q_{d_1}(0,t) + q_{d_2}(0,t),$$

where subscript p denotes the parent vessel and subscripts $d_i, i = 1,2$ denotes the two daughter vessels. The outflow from the large terminal arteries and the inflows to the corresponding large terminal veins are obtained by connecting arterial and venous structured trees. Finally, at the outflow of the large veins (at the inflow to the left atrium), we specify a constant pressure of 2 mmHg which corresponds to the normal mean pressure.

2.2 The small arteries and veins

In order to develop a model of the complete pulmonary circulation, we prescribe separate structured-tree models for the arterial and venous trees, extending Olufsen et al.'s (2000) model for the systemic circulation and Olufsen et al.'s (2012) model for the pulmonary circulation, and then join these two trees. Since the small pulmonary veins are known to follow closely the course of the pulmonary arteries, we modelled the pulmonary venous tree as a 'mirror image' of the pulmonary arterial tree depicted in Fig. 1. The two trees are represented by the same topology, assuming a one-to-one correspondence between each vessel, but vessels are allowed to have different length-to-radius ratios and material properties (e.g. compliances), from vessels in the mirror tree. To ensure that the same number of branches in arterial and venous trees, the radius of the root (i.e. largest) vessel must be the same for arterial and venous trees. Both the arterial and venous structured trees are set up, as described by Olufsen (1999) and Olufsen et al. (2000, 2012), assuming that at each junction the daughter vessel radius can be predicted from the parent vessels as $r_{d_1} = \alpha\, r_{\mathrm{p}}$ and $r_{d_2} = \beta\, r_{\mathrm{p}}$, i.e. for any vessel, the radius $r = \alpha^i \beta^j r_0$, where r_0 is the radius of the root vessel. Scaling factors α and β were determined from studies suggesting that branching of smaller arteries is governed by three relations: a radius relation, an asymmetry ratio γ and an area ratio η, given by

$$r_{\mathrm{p}}^{\xi} = r_{d_1}^{\xi} + r_{d_2}^{\xi}, \quad 2.33 \le \xi \le 3,$$
$$\gamma = r_{d_2}^2 / r_{d_1}^2,$$
$$\eta = \frac{r_{d_1}^2 + r_{d_2}^2}{r_{\mathrm{p}}^2} = \frac{1+\gamma}{(1+\gamma^{\xi/2})^{2/\xi}}, \quad \eta > 1,$$

where the subscript p refers to the parent vessel and subscripts $d_i, i = 1,2$ to the daughter vessels. It should be noted that only two of these relations are mathematically independent. The exponent ξ in the radius relation was obtained from considerations associated with minimising work in the arterial system. A value of $\xi = 3$ is optimal for laminar flow, $\xi = 2.33$ for turbulent flow and $\xi = 2.76$ is a good choice for arterial blood flow (Pollanen 1992; Suwa et al. 1963; Uylings 1977). Finally, the scaling factors α and β satisfy observations that the cross-sectional areas $A_{d_1}, A_{d_2} < A_{\mathrm{p}}$ while $A_{d_1} + A_{d_2} > A_{\mathrm{p}}$.

In addition to the radius relations, the length of each vessel must be specified. For the pulmonary vessels, a length-to-radius relation was obtained by analysing data summarised by Fung (1996) (based on experiments by Singhal et al. (1973)) combined with observations from more recent studies by Huang et al. (1996) that suggest a length-to-radius relation given by

$$l = \begin{cases} 15.75 r^{1.10} & \text{arterial radius } \ge 0.005\,\text{cm}, \\ 1.79 r^{0.47} & \text{arterial radius } \le 0.005\,\text{cm}, \\ 14.54 r & \text{venous radius } \le 0.2\,\text{cm}, \end{cases} \tag{5}$$

where the l and r (both specified in cm) denote the length and radius of the vessel.

The recent study by Cousins and Gremaud (2012) showed that the resistance predicted at the root of the structured trees critically depend on the value of the minimum vessel $r_{\min}$ at which trees are terminated. For the pulmonary arterial and venous structured trees, we chose $r_{\min} = 50\,\mu\text{m}$. This choice of cut-off value allows us to use a single Eq. $(5)_1$ within each

arterial tree and $(5)_3$ within the venous trees, to scale the vessels' lengths to their radii. Note that different scaling for the arteries and veins provides asymmetry between the two structured trees.

The flow and pressure predicted within the structured trees applied at the end of the large vessels is modelled to mimic dynamics within the vascular beds. These networks provide resistance to the flow and dampen the flow oscillations. The parameters, ξ, γ and $r_{\min}$ along with a given r_0, determine the size and density of the structured tree, and hence the total cross-sectional area through which the blood flows. Since we fix $r_{\min}$ instead of the number of generations, the total number of vessels in each structured tree attached to unique terminal vessels varies with r_0, providing non-uniform downstream resistances within different vascular beds. For instance, for $\xi = 2.76$, $\gamma = 0.41$, $r_{\min} = 0.005\,\text{cm}$ and $r_0 = 0.9\,\text{cm}$, the number of generations in α and β branches of the arterial side is 56 and 10, respectively, yielding 7.4×10^5 vessels in the tree. This changes to 49 and 9 generations in the α and β branches, respectively, with total number of vessels reducing to 5.8×10^5, if $r_0 = 0.45\,\text{cm}$. Moreover, it has been shown in Olufsen et al. (2012) that changing ξ and γ changes the structured-tree density, and hence the peripheral flow resistance.

2.2.1 Small-vessel fluid dynamics

As in the case of large vessels, three equations determine the flow, pressure and area for each vessel in the structured tree. However, for these small vessels, as in Olufsen et al. (2000), nonlinear effects are small, allowing linearisation of the governing equations. The linearised momentum equation is given by

$$\frac{\partial u}{\partial t} + \frac{1}{\rho}\frac{\partial p}{\partial x} = \frac{\nu}{r}\frac{\partial}{\partial r}\left(r\frac{\partial u}{\partial r}\right). \tag{6}$$

Assuming all quantities are periodic, pressure and flow can be expressed in the frequency domain using complex periodic Fourier series given by

$$p(x,t) = \sum_{k=-\infty}^{\infty} P(x,\omega_k)\mathrm{e}^{i\omega_k t}$$

$$\text{and } q(x,t) = 2\pi\int_0^{r_0} u(r,x,t)r\,\mathrm{d}r = \sum_{k=-\infty}^{\infty} Q(x,\omega_k)\mathrm{e}^{i\omega_k t},$$

where

$$u(r,x,t) = \sum_{k=-\infty}^{\infty} U(r,x,\omega_k)\mathrm{e}^{i\omega_k t}$$

and $\omega_k = 2\pi k/T$ is the angular frequency, with

$$P(x,\omega_k) = \frac{1}{T}\int_{-T/2}^{T/2} p(x,t)\mathrm{e}^{-i\omega_k t}\mathrm{d}t,$$

$$Q(x,\omega_k) = \frac{1}{T}\int_{-T/2}^{T/2} q(x,t)\mathrm{e}^{-i\omega_k t}\mathrm{d}t$$

and

$$U(r,x,\omega_k) = \frac{1}{T}\int_{-T/2}^{T/2} u(r,x,t)\mathrm{e}^{-i\omega_k t}\mathrm{d}t.$$

Thus for each value of ω_k, Eq. (6) becomes

$$i\omega U + \frac{1}{\rho}\frac{\partial P}{\partial x} = \frac{\nu}{r}\frac{\partial}{\partial r}\left(r\frac{\partial U}{\partial r}\right), \tag{7}$$

where for convenience, we drop the suffix k. Assuming that the small vessels do not taper, (7) can be solved to give

$$U = \frac{1}{i\omega\rho}\frac{\partial P}{\partial x}\left(1 - \frac{J_0(r w_0/r_0)}{J_0(w_0)}\right),$$

where $w_0^2 = i^3 w^2$, $w^2 = r_0^2\omega/\mu$ is the Womersley number, and $J_0(x)$ is the Bessel function of the first kind and zero order.

Defining the frequency domain volumetric flow rate in terms of velocity,

$$Q = 2\pi\int_0^{r_0} Ur\mathrm{d}r \Rightarrow i\omega Q = \frac{-A_0}{\rho}\frac{\partial P}{\partial x}(1 - F_J), \tag{8}$$

where

$$F_J = 2J_1(w_0)/w_0 J_0(w_0)$$

and $J_1(x)$ is the first-order Bessel function of the first kind.

The one-dimensional continuity equation for the small vessels is the same as for the large vessels. Using the tube law (4), the continuity Eq. (1) can be written as

$$C\frac{\partial p}{\partial t} + \frac{\partial q}{\partial x} = 0,$$

where C is the compliance, which can be approximated by linearising the tube law (4), giving

$$C = \frac{\partial A}{\partial p} = \frac{3A_0 r_0}{2Eh}\left(1 - \frac{3pr_0}{4Eh}\right)^{-3} \approx \frac{3A_0 r_0}{2Eh} \tag{9}$$

since $Eh \gg pr_0$. Assuming periodicity, the continuity equation becomes

$$i\omega C P + \frac{\partial Q}{\partial x} = 0. \tag{10}$$

Differentiating (10) with respect to x and substituting the result into (8) gives a wave equation of the form

$$\frac{\omega^2}{c^2}Q + \frac{\partial^2 Q}{\partial x^2} = 0 \quad \text{or} \quad \frac{\omega^2}{c^2}P + \frac{\partial^2 P}{\partial x^2} = 0, \tag{11}$$

where the wave propagation velocity is given by

$$c = \sqrt{A_0(1 - F_J)/\rho C}. \tag{12}$$

Solving (10) and (11) gives the flow and pressure in the frequency domain at any spatial position x along a vessel segment

$$Q(x, \omega) = a \cos(\omega x/c) + b \sin(\omega x/c) \tag{13}$$

$$\text{and } P(x, \omega) = i g_\omega^{-1} (b \cos(\omega x/c) - a \sin(\omega x/c)), \tag{14}$$

where a and b are constants, ω is the frequency and $g_\omega = \sqrt{C A_0(1 - F_J)/\rho}$.

2.3 Structured-tree matching conditions

In the one-sided pulmonary arterial model (Olufsen et al. 2012), an outflow boundary condition was obtained at the terminal of each large artery by computing the root impedance, defined as $Z(x, \omega) = P(x, \omega)/Q(x, \omega)$, for each structured tree. Since only the arterial side of the circulation was considered, defining a scalar impedance function $Z(0, \omega)$ at the proximal end, in terms of known impedance $Z(L, \omega)$ at the distal end of each vessel in the tree, was sufficient to recursively compute the root impedance. However, to connect the network of arterial and venous vessels, we need to define a relation between pressures and flows at both ends of each vessel, and consequently derive a boundary condition that match the pressures and flows at the terminals of large arteries and veins. To do so, we set up expressions determining the admittance of each structured tree, a 2×2 matrix $\mathbf{Y}(\equiv \mathbf{Z}^{-1})$ (Peskin 1961), relating pressure and flow at the outflow of each large terminal artery to pressure and flow at the inflow to the corresponding large terminal vein, as shown in Fig. 3.

Unlike the one-sided structured tree, in which prediction of the root impedance required a constant impedance applied at the terminal branches of the structured tree, for the two-sided tree, no specific values of pressure and flow relations are required at points arterial trees connect with venous trees. The only conditions needed to set up the admittance matrix are the junction conditions requiring continuity of pressure and conservation of volume flux. The total or root admittance is calculated by joining admittances in series and parallel as described in Algorithm 1 in Sect. 2.3.4.

2.3.1 Admittance matrix for a single vessel

Given the boundary flows $Q_1 = Q(0, \omega)$ and $Q_2 = Q(L, \omega)$ which are defined such that inflows are positive, the admittance matrix is obtained by relating the flows and pressures at the proximal ($x = 0$) and distal ($x = L$) ends of a vessel of radius r using Eqs. (13) and (14) yielding

$$\begin{pmatrix} Q_1 \\ Q_2 \end{pmatrix} = \frac{i g_\omega}{S_L} \begin{pmatrix} -C_L & 1 \\ 1 & -C_L \end{pmatrix} \begin{pmatrix} P_1 \\ P_2 \end{pmatrix}, \tag{15}$$

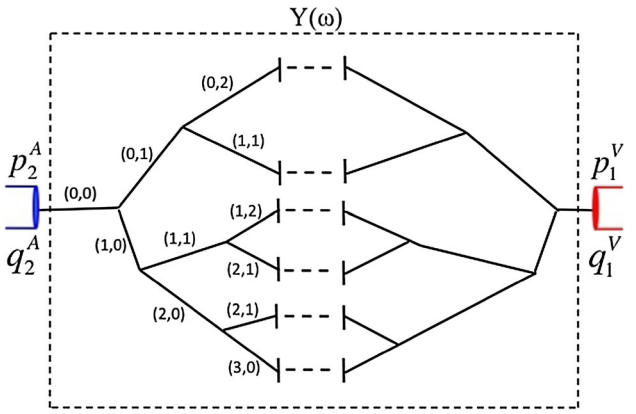

Fig. 3 Linking an arterial tree with a venous tree. For each vessel in the arterial tree, there is a mirror vessel in the venous tree which may have different compliance and length-to-radius ratio. The radii are defined as functions of root vessel radius via scaling factors α and β. Starting from terminals of structured trees, both trees are connected by joining the pairs of vessels in series and in parallel. Flows q_2^A and q_1^V, denote $q^A(L)$ (flow at distal end of large terminal arteries) and similarly $q^V(0)$ (flow at distal end of large terminal veins), respectively, and pressures p_2^A and p_1^V, represent $p^A(L)$ and $p^V(0)$, respectively. The flows are related to the pressures by a 2×2 admittance matrix $\mathbf{Y}(\omega)$. Note that the labels of branches are the ordered pairs, which refer to generation of vessel in the tree and are powers of scaling factors α and β, i.e. the label (i, j) indicates that the radius of the vessel is $\alpha^i \beta^j r_o$

where $C_L \equiv \cos(\omega L/c)$, $S_L \equiv \sin(\omega L/c)$, and

$$\mathbf{Y}(\omega) = \frac{i g_\omega}{S_L} \begin{pmatrix} -C_L & 1 \\ 1 & -C_L \end{pmatrix} \tag{16}$$

is the admittance matrix for any one artery or vein when $\omega \neq 0$. When $\omega = 0$, (15) becomes

$$\begin{pmatrix} Q_1 \\ Q_2 \end{pmatrix} = \frac{\pi r^4}{8\mu L} \begin{pmatrix} 1 & -1 \\ -1 & 1 \end{pmatrix} \begin{pmatrix} P_1 \\ P_2 \end{pmatrix} \tag{17}$$

and therefore

$$\mathbf{Y}(0) = \frac{\pi r^4}{8\mu L} \begin{pmatrix} 1 & -1 \\ -1 & 1 \end{pmatrix}, \tag{18}$$

which is the admittance matrix for $\omega = 0$. The derivation of (16) and (18) can be found in Vaughan (2010).

Non-dimensional admittance matrices In the frequency domain, pressure and flow are scaled using

$$P(x, \omega) = \rho g l \tilde{P}(x, \omega),$$
$$Q(x, \omega) = q_c \tilde{Q}(x, \omega),$$

where ρ is the density of blood, g is acceleration due to gravity, l is the characteristic length, q_c is the characteristic flow and $\tilde{P}$ and $\tilde{Q}$ are the non-dimensional pressure and flow, respectively. For a single vessel, these quantities allows computation of non-dimensional admittance $\tilde{\mathbf{Y}}$ given by

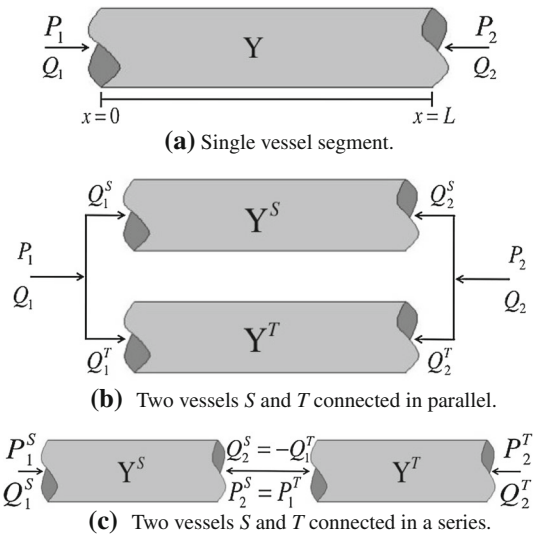

(a) Single vessel segment.

(b) Two vessels S and T connected in parallel.

(c) Two vessels S and T connected in a series.

Fig. 4 Relations between flow and pressure via admittance $\mathbf{Y}$, $\mathbf{Y}^{\parallel}$ and $\mathbf{Y}^{\Leftrightarrow}$ for a single vessel (**a**), vessels connected in parallel (**b**), and vessels connected in series (**c**). Q_1 and Q_2 are *positive* when the flows are *into* the vessel

$$\mathbf{Y}(x,\omega) = \frac{q_c}{\rho g l}\,\tilde{\mathbf{Y}}(x,\omega).$$

For convenience below, the tilde has been removed from all non-dimensional quantities.

2.3.2 Admittance matrix for two vessels in parallel

In the following, we consider two vessels, S and T, in parallel joined to a common inflow and outflow, as depicted in Fig. 4b. Since the pressure is continuous across a bifurcation, the pressure at the inlet to vessel S is the same as the pressure at the inlet to vessel T. Similarly, the pressure at the outlet of vessel S is the same as the pressure at the outlet of vessel T. Denoting the inlet and outlet pressures by P_1 and P_2, respectively, this connection can be described by

$$\begin{pmatrix} Q_1 \\ Q_2 \end{pmatrix} = \mathbf{Y} \begin{pmatrix} P_1 \\ P_2 \end{pmatrix}, \tag{19}$$

where Q_1 and Q_2 denote the inflow and outflow of the vessel, and $\mathbf{Y}$ is the admittance matrix. Volume flux is conserved across a bifurcation thus, for two vessels connected in parallel, the two admittances can be added giving

$$\begin{pmatrix} Q_1 \\ Q_2 \end{pmatrix} = \mathbf{Y}^{\parallel} \begin{pmatrix} P_1 \\ P_2 \end{pmatrix}, \quad \text{where} \quad \mathbf{Y}^{\parallel} = \mathbf{Y}^S + \mathbf{Y}^T \tag{20}$$

is the total admittance matrix for two vessels in parallel. The symbol $\parallel$ represents the admittance of two vessels connected in parallel.

2.3.3 Admittance matrix for two vessels in series

Next, we consider two vessels connected in series, as depicted in Fig. 4c. The flow and pressure can be written as

$$Q_k^i = \sum_{l=1}^{2} Y_{kl}^i\, P_l^i, \tag{21}$$

where $i = S, T$ and $k = 1, 2$ with Y_{kl} being the components of the 2×2 admittance matrix. Let $P = P_2^S = P_1^T$ along with $Q_2^S = -Q_1^T$ at the junction of two vessels in series. This system can be solved for P using (21), giving

$$\begin{pmatrix} Q_1^S \\ Q_2^T \end{pmatrix} = \mathbf{Y}^{\Leftrightarrow} \begin{pmatrix} P_1^S \\ P_2^T \end{pmatrix} \tag{22}$$

where

$$\mathbf{Y}^{\Leftrightarrow} = \frac{1}{Y_{22}^S + Y_{11}^T} \times \begin{pmatrix} \det(\mathbf{Y}^S) + Y_{11}^S Y_{11}^T & -Y_{12}^S Y_{12}^T \\ -Y_{21}^S Y_{21}^T & \det(\mathbf{Y}^T) + Y_{22}^S Y_{22}^T \end{pmatrix} \tag{23}$$

is the admittance matrix for two vessels connected in series. Here, the symbol $\Leftrightarrow$ denotes the admittance matrix of vessels joined in series.

2.3.4 Linking an arterial and a venous tree

To link the arterial and venous trees, the two trees should be 'mirror images' of each other in as much as that they should have the same number of bifurcations and terminal vessels; however, each tree is allowed to have different vessel properties including compliance and length-to-radius ratio. The admittance matrix (16) is computed for each individual vessel, and the total admittance of the two connected trees is found recursively by combining the admittance matrices of vessels and subtrees in series [using (23)] and in parallel [using (20)] as appropriate. To set up the recursion algorithm, each pair of vessels (arterial and venous) are assigned an index (i, j) indicating that the radius of the vessel is $\alpha^i \beta^j r_o$; in addition each vessel is assigned a label "A" or "V" specifying if the vessel is an artery or a vein. For example, the total admittance for a small network consisting of an arterial (A) and a venous (V) tree, each having one bifurcation with branches scaled by factors α and β, is given by

$$\begin{aligned} \mathbf{Y} &= \mathbf{Y}^A(0,0) \\ &\Leftrightarrow [\{\mathbf{Y}^A(1,0) \Leftrightarrow \mathbf{Y}^V(1,0)\} \parallel \{\mathbf{Y}^A(0,1) \Leftrightarrow \mathbf{Y}^V(0,1)\}] \\ &\Leftrightarrow \mathbf{Y}^V(0,0). \end{aligned}$$

Below we describe the general algorithm valid for trees where the compliance is identical for arterial and venous vessels, while the length-to-radius ratio is larger for vessels in the venous tree.

Algorithm 1: Recursive algorithm to compute the 2×2 admittance matrix $\mathbf{Y}$ *for a connected network of arterial and venous vessels*

The root admittance matrix Y is computed recursively by calling Y = admit(0,0).

Recursive function $\mathrm{Y}(i,j) = \mathrm{admit}(i,j)$

if $r(i+1,j) < r_{min}$ (α-branch)
  for k = A, V
    $\mathrm{Y}^k(i+1,j) =$ eqn (16), $\quad \omega \neq 0$
    $\mathrm{Y}^k(i+1,j) =$ eqn (18), $\quad \omega = 0$
  end
  $\mathrm{Y}(i+1,j) = \mathrm{ser}(\mathrm{Y}^A(i+1,j),\mathrm{Y}^V(i+1,j))$
else
  $\mathrm{Y}(i+1,j) = \mathrm{admit}(i+1,j)$
end

if $r(i,j+1) < r_{min}$ (β branch)
  for k = A, V
    $\mathrm{Y}^k(i,j+1) =$ eqn (16), $\quad \omega \neq 0$
    $\mathrm{Y}^k(i,j+1) =$ eqn (18), $\quad \omega = 0$
  end
  $\mathrm{Y}(i,j+1) = \mathrm{ser}(\mathrm{Y}^A(i,j+1),\mathrm{Y}^V(i,j+1))$
else
  $\mathrm{Y}(i,j+1) = \mathrm{admit}(i,j+1)$
end

$\mathrm{Y}_{mid}(i,j) = \mathrm{Y}(i+1,j) + \mathrm{Y}(i,j+1)$

for k = A, V
  Y^k(i,j) = eqn (19), $\quad \omega \neq 0$
  Y^k(i,j) = eqn (20), $\quad \omega = 0$
end

$\mathrm{Y}(i,j) = \mathrm{ser}(\mathrm{ser}(\mathrm{Y}^V(i,j),\mathrm{Y}_{mid}(i,j)),\mathrm{Y}^A(i,j))$

Series function $\mathrm{Y}(i,j) = \mathrm{ser}(\mathrm{Y}^S(i,j),\mathrm{Y}^T(i,j))$

For vessel (i,j) compute determinants

$$D^k = \mathrm{Y}^k_{11}\,\mathrm{Y}^k_{22} - \mathrm{Y}^k_{12}\,\mathrm{Y}^k_{21}, \quad k = S,T$$

then Y has components

$$\mathrm{Y}_{11} = (D^S + Y^S_{11}\,Y^T_{11}) / (Y^S_{22} + Y^T_{11})$$
$$\mathrm{Y}_{12} = (-Y^S_{12}\,Y^T_{12}) / (Y^S_{22} + Y^T_{11})$$
$$\mathrm{Y}_{21} = (-Y^S_{21}\,Y^T_{21}) / (Y^S_{22} + Y^T_{11})$$
$$\mathrm{Y}_{22} = (D^T + Y^S_{22}\,Y^T_{22}) / (Y^S_{22} + Y^T_{11}).$$

2.4 Vessel compliance

Only a few studies (Greenfield and Douglas 1963; Yen and Sobin 1988; Yen et al. 1990; Krenz and Dawson 2003; Reeves et al. 2005) provide quantitative data on the elastic properties of human pulmonary arteries and veins. In our previous study (Olufsen et al. 2012), a value for the pulmonary arterial compliance parameter C in (9) was derived from the work of Krenz and Dawson (2003), who measured a stiffness parameter λ given by

$$D/D_0 = 1 + \lambda p, \tag{24}$$

where p denotes the transmural pressure (mmHg), D (cm) the vessel diameter associated with pressure p, and, D_0 the vessel diameter at zero pressure $p = 0$. They suggested that a diameter-independent, constant value of $\lambda = 0.02\,\mathrm{mmHg}^{-1}$ holds throughout the pulmonary arteries and veins, implying a uniform compliance across the entire pulmonary system (see Figure 7 in Krenz and Dawson 2003). Inserting λ into the tube law (4) gives

$$Eh/r_0 = 3/4\lambda = 37.5\,\mathrm{mmHg}. \tag{25}$$

This value is approximately 17 times smaller than the stiffness parameter value ($8.65 \times 10^5\,\mathrm{g\,s^{-2}\,cm^{-1}}$) used by Olufsen et al. (2000) for systemic arteries. However, several studies (Evans et al. 1960; Greenfield and Douglas 1963; Patel et al. 1962) have reported that the compliance of the pulmonary arteries is larger by a factor of 2–10 times the systemic arterial compliance. This is significantly less than the factor of 17 suggested by Krenz and Dawson (2003). As reported in our previous study dealing only with the pulmonary arterial tree (Olufsen et al. 2012), albeit for a different outflow condition, this value of λ leads to low arterial pulmonary pressures (3–14 mmHg), whereas typical pulmonary arterial pressures should range from 10–25 mmHg (Fung 1996; Hall 2011). The very small compliance proposed by Krenz and Dawson was extracted from a set of measurements collated from 26 studies, on six different species, conducted in vivo and in vitro. However, the mechanical properties of vessels are known to change when excised (Valdez-Jasso et al. 2009).

Simulations by Clipp and Steele (2009) support using a larger compliance value, about three times the arterial value, which is scaled with vessel radius, and they discuss the sensitivity of modelling results to the stiffness parameter. However, several authors (Attinger 1963; Krenz and Dawson 2003; Yen et al. 1990) believe that the pulmonary compliance is diameter-independent and hence spatially invariant across the entire system. Attinger (1963) supports this hypothesis in a study showing that the pulse wave speed in the pulmonary arteries does not increase away from the heart.

By analysing data from arterial and venous vessels of several orders of magnitude in diameter, Krenz and Dawson (2003) provide strong evidence that the compliance is constant across the system. Finally, the independent study on *excised* human lungs by Yen et al. (1990), defines averaged compliance values of $\lambda_A = 0.012 \pm 0.0024\,\mathrm{mmHg}^{-1}$

for arterial vessels with diameters 200–1,600 μm and $\lambda_V = 0.013 \pm 0.0064\,\text{mmHg}^{-1}$ for venous vessels with diameters ranging from 100–1,200 μm. This suggests that the overall compliance does not differ significantly between the pulmonary arterial and venous trees. Consequently, we use a constant compliance,

$$\frac{Eh}{r_0} = 195\,\text{mmHg} \quad (\approx 26\,\text{kPa}), \tag{26}$$

that is approximately the same as the value used by Clipp and Steele (2009, 2012), for pulmonary arteries. This value gives simulated pressure waveforms consistent with the physiological ranges of 8.8±3.3–22±4.2 mmHg (Greenfield and Douglas 1963; Herve et al. 1989), 10–25 mmHg (Fung 1996) and 8–25 mmHg (Hall 2011) in the proximal pulmonary arteries.

2.5 Numerical methods

As in our previous studies (Olufsen 1999; Olufsen et al. 2000, 2012), we use a two-step Lax–Wendroff scheme to compute volume flux and area in the large pulmonary arteries and veins. The implementation of the bifurcation and inflow conditions is identical to the methods described previously (for details, see Appendices A.1 and A.2 of Olufsen 1998). New for this study is the matching condition (19) needed to link arterial and venous trees.

This is transformed to the time domain using convolution, giving

$$q_k(t) = \sum_{l=1}^{2} \int_0^T y_{kl}(\tau)\, p_l(t-\tau)\, \mathrm{d}\tau, \quad k = 1, 2, \tag{27}$$

where $q_1(t)$ and $p_1(t)$ are the volume flux and pressure at the root of the arterial tree, and $q_2(t)$ and $p_2(t)$ are the volume flux and pressure at the root of the venous tree. $y_{kl}(t)$ is the inverse Fourier transform of $Y_{kl}(\omega)$. Equation (27) is the matching boundary condition to be applied at the end of terminal arteries and veins. Further details can be found in Appendices A.3 and A.4 of Vaughan (2010).

2.6 Mean pressure across small arteries and veins

By using the admittance matrix computed in Sect. 2.3.4, the mean pressure can be computed (for $\omega = 0$) along the connected trees representing arterioles and venules. To do so, it is necessary first to compute the pressures at the terminals of large vessels P_2^A and veins P_1^V for $\omega = 0$. These pressures can be extracted from (27) and assigned to the root of the structured arterial and venous trees as

$$P_1^A(0,0) = P_2^A \quad \text{and} \quad P_2^V(0,0) = P_1^V,$$

where $P_k^A(0,0)$ and $P_k^V(0,0)$ denote the pressures at the roots of the structured trees. The corresponding flows can be found from

$$\mathbf{Q}(0,0) = \mathbf{Y}(0,0)\,\mathbf{P}(0,0), \tag{28}$$

where $\mathbf{Q} = [Q_1^A \;\; Q_2^V]^T$ and $\mathbf{P} = [P_1^A \;\; P_2^V]^T$.

For each vessel, the pressure at distal ends of arterial and venous root vessels can be computed as

$$P_k^S(0,0) = P_l^S(0,0) - R^S(0,0)\, Q_l^S(0,0), \tag{29}$$

Where

$$R^S = \frac{8\mu L^S}{\pi r^S} \frac{q_c}{\rho g l}$$

and $(k,l) = (2,1)$ if $S = A$ and $(k,l) = (1,2)$ if $S = V$.

Pressure drop along $\boldsymbol{\alpha}$ *and* $\boldsymbol{\beta}$ *pathways*

Suppose that there is a maximum of n generations along α branches from the root vessel, i.e. vessels scaled by $\alpha^i \beta^0$, $i = 1, \ldots, n$. Then, following similar steps as those for the root vessel, one may compute pressure and flow in any vessel segment along the α branch. So for any vessel indexed $(i, 0)$ in the tree, continuity of pressure gives

$$P_l^S(i,0) = P_k^S(i-1,0), \tag{30}$$

where $(k,l) = (2,1)$ if $S = A$ and $(k,l) = (1,2)$ if $S = V$. Again, the flows can be computed from

$$\mathbf{Q}(i,0) = \mathbf{Y}(i,0)\,\mathbf{P}(i,0), \tag{31}$$

where $\mathbf{Y}(i,0)$ is the admittance matrix involving all the vessels of and between generations $\alpha^i \beta^0$. Finally, the pressure at the distal end of every vessel is given by

$$P_k^S(i,0) = P_l^S(i,0) - R^S(i,0)\, Q_l^S(i,0). \tag{32}$$

In a similar way, one may compute the pressure along the β branch with m generations.

Pressure in vessels at all generations For any other generation vessel in the connected trees, the pressure continuity in the case of α parentage implies that

$$P_l^S(i,j) = P_k^S(i-1,j)$$

and if the vessel has β parentage then

$$P_l^S(i,j) = P_k^S(i,j-1),$$

where $i = 1, \ldots, n$ and $j = 1, \ldots, m$ and l, k are defined for vessel S. The flows at the respective ends are given by

$$\mathbf{Q}(i,j) = \mathbf{Y}(i,j)\,\mathbf{P}(i,j).$$

Finally, the pressures at the distal end of any vessel in the tree can be computed from

$$P_k^S(i,j) = P_l^S(i,j) - R^S(i,j)\, Q_l^S(i,j).$$

Below we give the recursive algorithm for computing mean pressure across α and β branches for the complete structured trees.

Algorithm 2: Mean pressure along α branches

Result: PMEAN

Input: Terminal $p_2^A(t)$ and $p_1^V(t)$

Apply FFT (fast Fourier transform)

$$P_2^A(\omega) = \mathrm{FFT}(p_2^A(t))$$
$$P_1^V(\omega) = \mathrm{FFT}(p_1^V(t))$$

if $\omega = 0$
For each vessel (i,j), $i = 0,\ldots,n$, $j = 0,\ldots,m$.
  $\mathrm{comp}(i,j,:,:) = \mathrm{Y}(i,j)$

for $i = 0 : n$
  if $(i = 0)$
    $P_1^A(i,0) = P_2^A$
    $P_2^V(i,0) = P_1^V$
  else
    $P_1^A(i,0) = P_2^A(i-1,0)$
    $P_2^V(i,0) = P_1^V(i-1,0)$
    $\mathrm{Y}(i,0) = \mathrm{comp}(i,0,:,:)$
  for $(S,k) = (A,1)$ and $(V,2)$
    $Q_k^S(i,0) =$ eqn (31)
  for $(S,k) = (A,2)$ and $(V,1)$
    $P_k^S(i,0) =$ eqn (32)
end

Apply IFFT (inverse fast Fourier transform)

$$(\mathrm{PMEAN})_2^A(t) = \mathrm{IFFT}(P_2^A(0))$$
$$(\mathrm{PMEAN})_1^V(t) = \mathrm{IFFT}(P_1^V(0))$$

3 Results

3.1 Normal case

We first show results for a healthy young subject, whose measured vessel diameters are given in Table 1, followed by results for pulmonary hypertension. While vessel geometries and inflow into the MPA were partially obtained from measurements, other quantities such as density, viscosity and scaling ratios were determined from literature values. Flow and pressure results for the healthy young subject are shown in Fig. 5. This figure shows the predicted flows and pressure from three locations along the MPA, LPA, RPA, RIV, RSV and LIV. The first column shows that the pressure in the large arteries ranges from 10 to 25 mmHg. Slight differences in peak pressure and arrival time for the reflected waves can be observed between proximal and distal ends of the MPA and RPA, while no significant differences can be observed in the LPA. The second column shows the venous pressure dynamics. The magnitude and variation in pressure remain low in the veins. The pressures are biphasic (have two maxima) and the LIV pressure oscillates about 2 mmHg, the constant right atrial pressure specified in the model. In the RIV and RSV, the pressure remains above 2 mmHg. As for the arteries, there is little change in flow with distance along individual vessels, but the differences in geometry between the left- and right-sided vessels lead to a greater flow in the LIV than in the RIV and RSV.

Figure 6 shows the mean (time-averaged over one cardiac cycle) pressure drop across the arterial and venous vascular beds connecting the RIA and RIV. The results are similar for the other vascular beds. The first two panels depict the pressure at the root of the arterial and venous trees. These pressures are imposed as boundary conditions and used to compute the mean pressure drop along the small vessels connecting the RIA to the RIV. The last panel shows the mean pressure drop across the combined arterial and venous beds. The mean pressures are plotted along the α branch (composed of vessels scaled by $\alpha^i\beta^0$, $i = 1,\ldots,n$), the β branch (composed of vessels scaled by $\alpha^0\beta^j$, $j = 1,\ldots,m$ where $m < n$), and the average computed over all branches of the same radius. The scale used for the radius r is logarithmic ($\log_{10} r$), ranging from the largest to smallest arteries and then from the smallest to largest veins.

Along the arterial tree, the pressure drops from about 17–10 mmHg, and along the venous tree the pressure continues to decrease from about 10–2 mmHg. It should be noted that the pressure drops differ significantly between the two extreme cases: on the arterial side, pressures in the β branches are greater than those in the α branches, and vice versa on the venous side. For the α branches, the greatest pressure drop occurs in the larger arteries and veins, whereas the opposite holds for the β branches.

3.2 Pulmonary hypertension

Pulmonary hypertension is a rare condition, with less than 50 cases per million people (Peacock et al. 2007). However, its occurrence is significantly higher for at-risk patient groups including HIV patients (Hachulla et al. 2005; Sitbon et al. 2008), patients with systemic sclerosis (Mukerjee and George 2003), and with sickle cell disease (Fonseca et al. 2012; Machado and Gladwin 2010). Moreover, the consequences of the disease for those affected are often severe. The condition may arise as the result of multiple mechanisms, and as a result, the disease is often divided into subcategories (Peacock and Rubin 2004; Simonneau et al. 2004). While a large number of specific subcategories exist, in this study, we analyse the effect of pulmonary hypertension according to three major subgroups characterised by observed anatomical changes of the blood vessels. These include as follows:

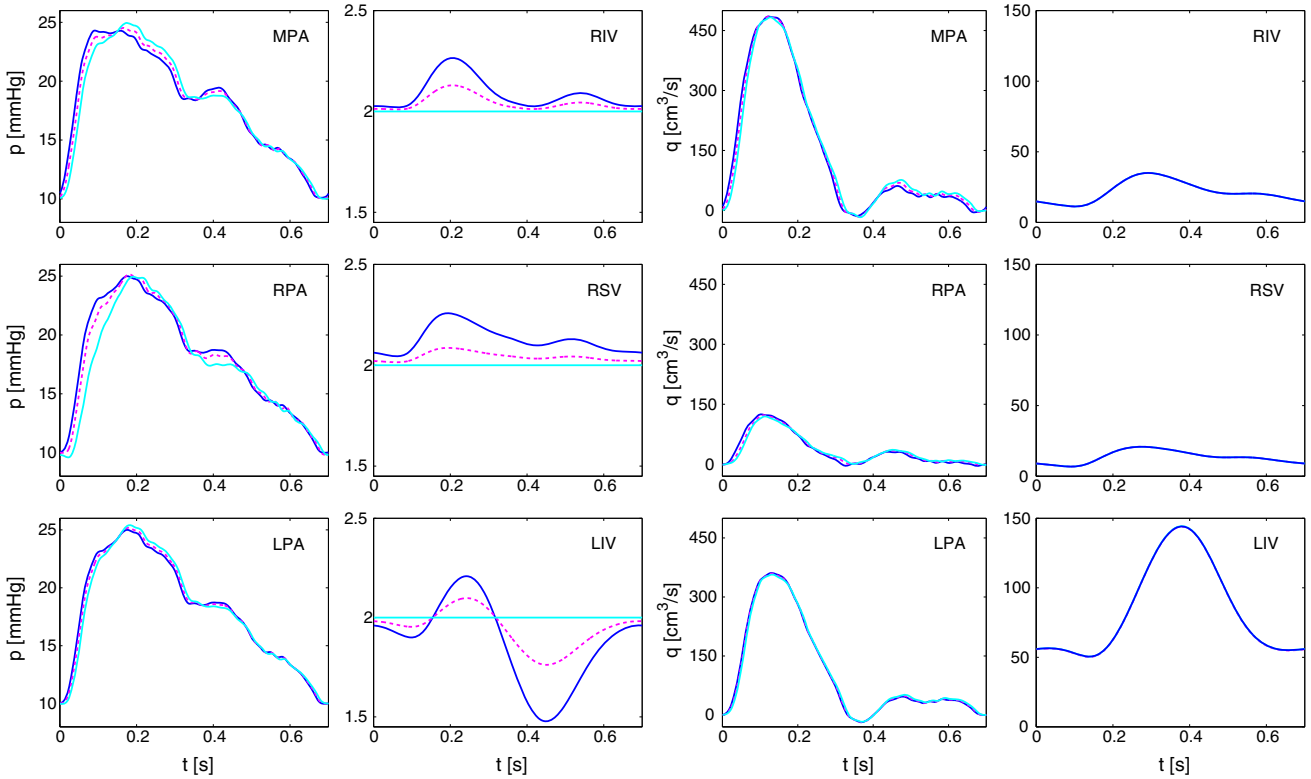

Fig. 5 Predicted pressure (first *two columns*) and flow (last *two columns*) at three locations along the large arteries (MPA, RPA, and LPA) and veins (RIV, RSV and LIV). For each vessel, flow and pressure are evaluated at the vessel inlet (*solid blue*), at the midpoint (*dashed magenta*), and at the end (*solid cyan*)

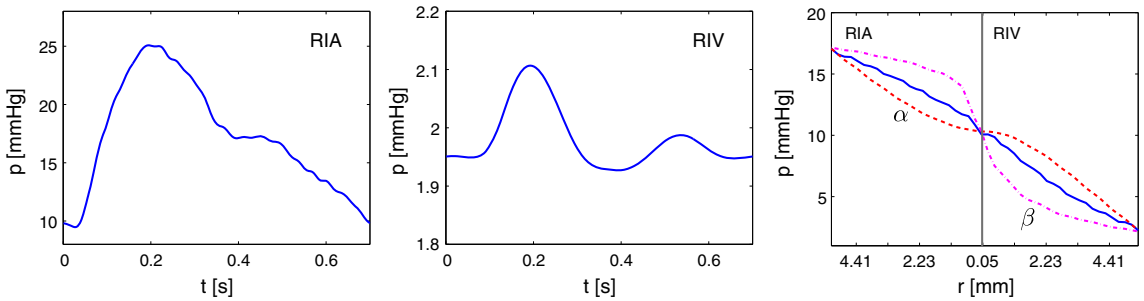

Fig. 6 Pressure profiles in a typical vascular bed. The first two graphs give pressures at the roots of the vascular bed connecting the RIA and RIV. The last graph shows mean pressure changes along the α and β pathways, together with the mean over all vessels of the same radius. The mean (time-averaged) pressure is plotted against vessel radius on a linear-log scale. The pressure drop across the α branch is marked by a *dashed red line*, the β branch pressure drop is marked by a *dashed-dot magenta line*, and across all the branches of the same radius by a *solid blue line*

Group I: Pulmonary arterial hypertension (PAH) This group of conditions includes pathophysiology observed in patients with increased stiffness and resistance of small pulmonary vessels of diameters $<500\,\mu$m (Lankhaar et al. 2006; Reeves et al. 2005).

Group II: Pulmonary hypertension associated with hypoxic lung disease (HLD) This pathophysiology is associated with vascular remodelling, typically affecting vessels with a diameter $<500\,\mu$m. In particular, it has been reported that patients with HLD have a reduced density of vessels within the pulmonary vascular bed (vascular rarefaction). This type of remodelling is observed in patients with an underlying respiratory disease (Tuder et al. 2007).

Group III: Chronic thromboembolic pulmonary hypertension (CTEPH) For patients with this form of hypertension, the problem is initially located in larger vessels, which display decreased vessel diameter and increased stiffness. Eventually, the condition may propagate and also affect small pul-

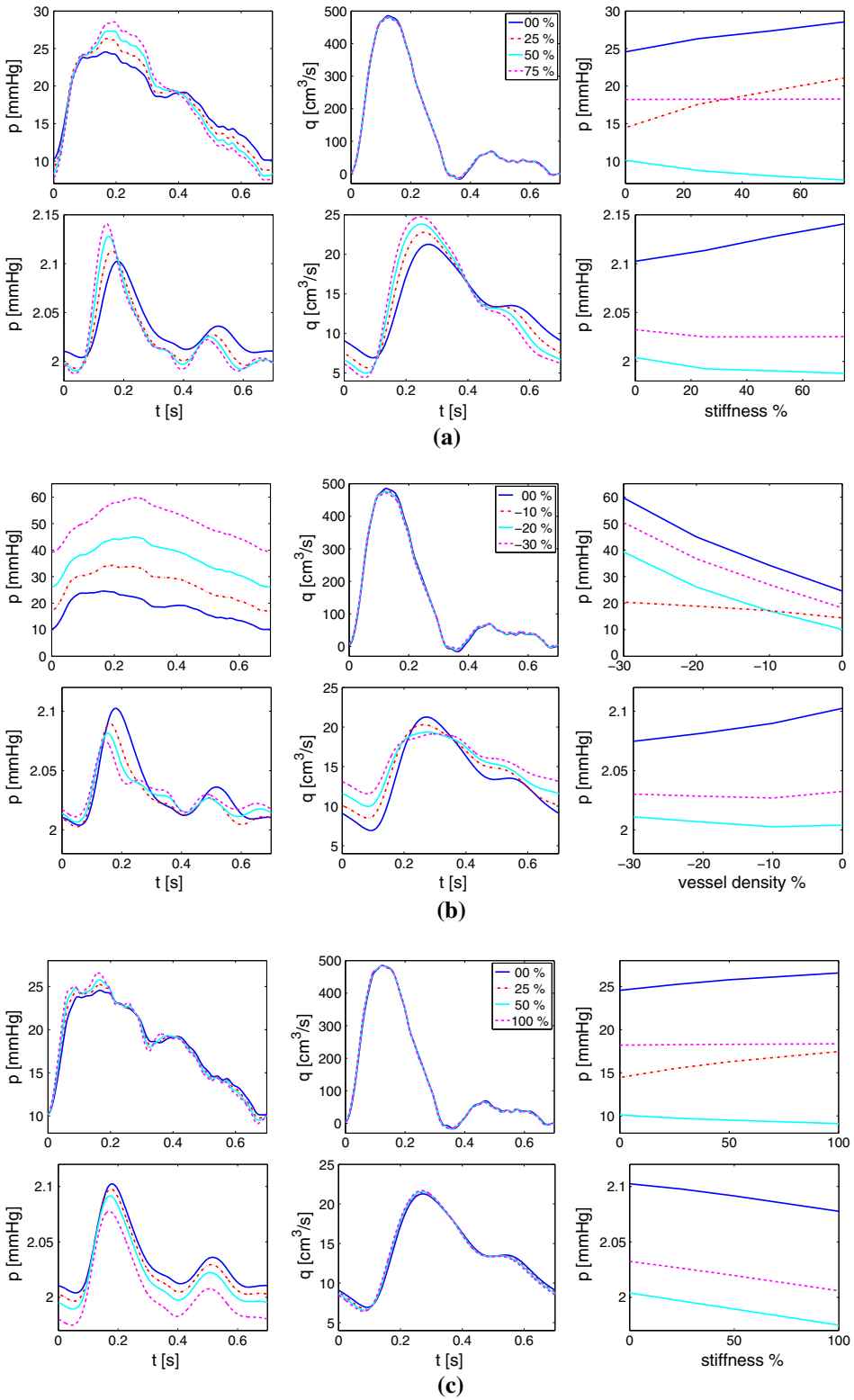

Fig. 7 Effect of hypertension on pressure and flow at midpoints of the MPA and RSV. The first two columns show pressure and flow waveforms. The third column gives peak (*solid blue*), mean (*dashed magenta*), pulse (*dashed-dot red*) and trough (*solid cyan*) pressures. **a** Group I: effects of PAH in the MPA (*top row*) and RSV (*bottom row*). The legend shows the % increase in the small-vessel stiffness. **b** Group II: effects of vascular remodelling due to HLD in the MPA (*top row*) and RSV (*bottom row*). The legend shows the % decrease in the vascular density of the structured trees. **c** Group III: effects of CTEPH in the MPA (*top row*) and RSV (*bottom row*). The legend shows the % increase in the large vessel stiffness

monary vessels as observed for patients with PAH (Castelain et al. 2001; Dartevelle et al. 2004).

The results of computations simulating these three disease classes are shown in Fig. 7 and summarised below.

3.2.1 Pulmonary arterial hypertension (PAH)

Pulmonary arterial hypertension can be triggered by a variety of pathologies (Barst et al. 2004), but an underlying feature of

the condition is the stiffening of the smaller pulmonary arteries. Reeves et al. (2005) showed that the arterial distensibility is decreased in healthy ageing and in patients with chronic hypoxia, and that reduced distensibility leads to increased stiffening of the small vessels. In this study, the reduction in distensibility is modelled by increasing the stiffness parameter Eh/r_0, which is inversely proportional to the distensibility parameter, up to 100 % for the large arteries and 75 % for the small blood vessels.

Figure 7a shows the effects of small-vessel stiffening within the arterial and venous structured trees on predicted pressures at midpoints in the MPA and RSV. In the MPA, the increased stiffness results in an increase in peak and pulse (the peak minus trough) pressure, and amplified oscillations of the pulmonary venous pressure and flow waveforms, with little change in the flow through the MPA. The increased small-artery stiffness results in a delay of the peak pressure wave arrival.

3.2.2 *Pulmonary hypertension associated with hypoxic lung disease (HLD)*

Hypoxic lung disease results in hypoxic pulmonary vasoconstriction, microvascular rarefaction and vascular remodelling (Tuder et al. 2007), all of which contribute to pulmonary hypertentsion that aggravates the hypoxaemia already present. Here, we focus on vascular rarefaction and its contribution to pulmonary hypertension. In Olufsen et al. (2012), rarefaction within the systemic arterial vascular beds was modelled by reducing the radius exponent ξ and the asymmetry ratio γ. Decreasing these parameters results in a decrease in the area ratio η within the structured tree. This approach is extended here to study the reduction in area ratios within both arterial and venous structured trees. For a typical structured tree, the effects of changing the vascular density ξ in a neighbourhood of the normal physiological values ($\xi_{\text{normal}} = 2.76$) are given in Table 2.

Table 2 The effects of changing radius exponent ξ on the vascular density within the vascular beds

ξ	No. of vessels $\times 10^5$	% change
2.40	4.6	−27
2.50	5.1	−20
2.60	5.6	−12
2.76	6.3	0
2.90	7.1	+12
3.00	7.7	+22

The deviation in the total number of small vessels from normal values is presented for the arterial structured tree connected to the RIA. The minus sign indicates a reduction in density while a plus indicates an increase

Figure 7b shows predicted pulse pressure waveforms in the MPA. Rarefied vascular beds result in a significant increases in peak, trough and mean arterial pressures. Further, as the degree of rarefaction is increased, the separate peaks from the incident and reflected pressure pulses merge forming a single, more featureless, peak in the pressure waveform. This figure also illustrates the effects of rarefaction on the pulmonary veins, where the amplitude of the pressure and flow waveforms is reduced. In addition, rarefaction causes a phase shift in the venous pulse waves, with both venous pressure and flow waveforms peaking earlier.

Figure 8 illustrates how the small-vessel remodelling (HLD) affects the pressure drop across the vascular bed connecting the RIA and RIV. Most significantly, the increased pressure at the inlet to the vascular bed raises the overall pressure in both the small arteries and veins. In particular, the arteries in branches that decrease rapidly in radius with generation number, such as the β branch illustrated in the last panel, experience higher pressures than average for their radius making them even more susceptible to further injury and disease.

3.2.3 *Chronic thromboembolic pulmonary hypertension (CTEPH)*

The pathophysiology associated with chronic thromboembolic pulmonary hypertension is similar to that of pulmonary arterial hypertension, except that it occurs in the large proximal pulmonary arteries (Castelain et al. 2001; Dartevelle et al. 2004), although the small vessels may also be affected eventually. As in Sect. 3.2.1, in which PAH was studied, we simulate the initial effects of CTEPH by stiffening just the large arteries by up to twice as much as normal. The later involvement of small vessels is modelled by uniformly stiffening the walls of the large arteries and all of the small arteries and veins in the vascular beds.

Figure 7c shows the effect of increasing the stiffness of the large pulmonary arteries. Results show an increase in peak and pulse pressure, with a steeper earlier pressure peak followed by secondary pressure peak appearing shortly after the first peak. The increase in pressure and appearance of a second peak agrees with observations of pressure pulses in patients with chronic thromboembolic pulmonary hypertension by Lankhaar et al. (2006), although the observed increase in peak pressure is much greater than our predictions. Predicted flows in the MPA show negligible effects with increased stiffness. In the pulmonary veins, increased stiffness of the large arteries leads to a slight decrease in the amplitude of the pressure waveform and a slight increase in flow waveform without any notable changes in the shape of the waveforms. Finally, results with uniform stiffening of both large and small vessels were almost identical to those obtained for PAH, see Fig. 7a, which caused a significant

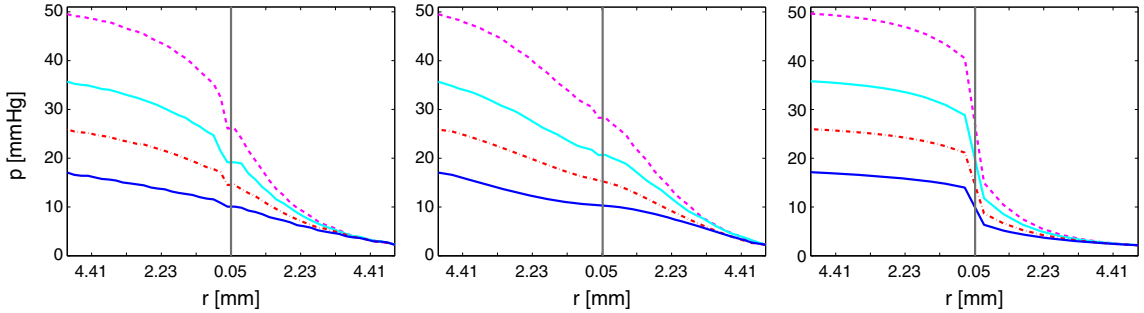

Fig. 8 Effects of pulmonary hypertension associated with hypoxic lung disease on mean pressure in vessels connecting the RIA with the RIV. Mean pressure is plotted against vessel radius on a linear-log scale. The *curves* correspond to a reduction in vascular density: normal (*solid blue*), 10 % decrease (*dashed-dot red*), 20 % decrease (*solid cyan*) and 30 % decrease (*dashed magenta*). The first column shows the pressure averaged over all vessels of the same radius, the α branch is plotted in the second column, and the β branch in third column. The pressures at the the roots of the RIA and RIV (*solid blue*) in the case of HLD, c.f. Fig. 7b, are imposed as boundary conditions

increase in arterial pressure and earlier peaking of the pressure pulse. These results agree well with observations by Lankhaar et al. (2006).

4 Discussion of results

The objective of this study is to simulate propagation of pressure and flow wave forms in the pulmonary circulation, by setting up a network including both small and large arteries and veins enabling simulation of blood flow and pressure along the complete path emanating at the right ventricle and ending at the left atrium. This was achieved by extending the structured-tree models (Clipp and Steele 2009; Olufsen et al. 2000, 2012) developed for simulation within arterial networks to include confluent venous networks. To do so, a set of matching boundary conditions was developed that relates the pressure and outflow from large arteries with the pressure and inflow into large veins. These are obtained by replacing the input impedance (Z) at the root of a structured tree by an admittance (a 2×2 matrix $\mathbf{Y}$) that links the two root vessels. Parameters for the pulmonary arteries are similar to those in Olufsen et al. (2012) and Vaughan (2010), except that the compliance parameter has been modified to improve pressure predictions. Finally, in order to understand the haemodynamics of the small blood vessels and the contribution of pulmonary venules towards total vascular resistance, the model was augmented to predict the mean pressure drop across both arterial and venous vascular beds.

It is worth mentioning that the root impedance gives a measure of total resistance to pulsatile flow in the vascular beds, which is analogous to the resistance in an electric circuit with alternating current. On the other hand, for electrical circuits, the admittance is defined as the inverse of impedance ($Y \equiv Z^{-1}$) and therefore provides the measure of how easily the current flows through the circuit. Although these analogies contribute in understanding the blood flow through resistance vessels and their effects on overall haemodynamics, the actual utility of admittance $\mathbf{Y}$ in this model is to enable us to relate the pressure and flow at the two ends (proximal and distal) of the vessel (see Eq. 19) in the periodic regime, and consequently at both ends of the circulation (the arterial and venous sides). This approach results into two convolution integrals describing the arterial-venous haemodynamic matching in the time domain.

After developing a computational solver, we presented simulations predicting normal pressure and flow dynamics for a healthy young male. These simulations give physiologically accurate pressure waveforms, c.f. panels in column 1 of Fig. 5 reporting pressures ranging from 10–25 mmHg in the large proximal arteries. These values agree with values reported by Fung (1996) (10–25 mmHg) and Hall (2011) (8–25 mmHg and $p_{\text{mean}} = 16$ mmHg). Moreover, the physiological pressures in the MPA and RPA are also in close agreement with values reported by Greenfield and Douglas (1963) (8.1–21$\pm$3.2 mmHg in the MPA) and Herve et al. (1989) (23.2$\pm$4.7–9.4$\pm$3.4 mmHg in the RPA). In addition, comparison of the pressure profile in the MPA, panel 1 of Fig. 5, with the pressure and radius pulsation graph reported in Figure 2 in Greenfield and Douglas (1963) shows that the shape of the pressure waves are similar. Both results include a pronounced dicrotic notch and a steep pressure rise in systole. This is a major improvement from our previous model of pulmonary arteries (Olufsen et al. 2012), which, using the same inflow boundary condition, simulates a rather featureless pressure waveform at a significantly low pressure (2–14 mmHg) (Figure 7a in Olufsen et al. 2012).

An increase in pressure is quite visible in distal MPA and LPA, which suggest that vessel tapering plays a role despite the fact that pulmonary vessels are more compliant and shorter compared with their systemic counterparts. In the case of LPA, we observe limited effects of wave propagation because the LPA is short (2.5 cm). Also, since tapering is minimal and no side branches are included within these

three vessels, the flow does not vary significantly among the three locations within each vessel. However, a significantly greater flow enters the LPA compared with the RPA, because the diameter of the LPA in this subject is significantly larger than the RPA (1.8 vs. 2.2 cm). Similarly, the flow through the LIV is much larger than through the other veins, since the LIV is connected to the LIA, which has a large distal diameter (1.8 cm), and since the way in which we have constructed the structured-tree model for the vascular beds requires the distal diameters of pairs of large arteries and veins to be the same. The geometry may also explain different oscillatory pressure behaviour observed in this vessel.

As suggested by Gao and Raj (2005), mean pressure predictions along pulmonary arteries and veins can be used to study the contribution of the small pulmonary veins towards the total peripheral resistance and haemodynamic regulation. Not only does the blood pressure continue to drop across the convergent tree of small veins (Fig. 6), but the decrease is slightly greater across the venous tree compared with the arterial tree (8 vs. 7 mmHg). Since both trees are topologically equivalent and mirror images with same number of vessels in each tree, it is the different length-to-radius ratios that are responsible for this difference. There is close agreement with results reported by Zhuang et al. (1983), who studied the haemodynamics of cat pulmonary vessels and reported that veins contribute approximately 49% of the total pulmonary vascular resistance.

In order to analyse the clinical applications of our model, we extended our model to simulate three cases of pulmonary hypertension including PAH, HLD and CTEPH. In PAH, the dicrotic notch tends to disappear and the peak and pulse pressures increase with the severity of the condition. These qualitative observations agree with observations by Lankhaar et al. (2006) who compared a control group with data from patients with idiopathic pulmonary hypertension. Similarly, the increase in pressure and the appearance of a second peak under CTEPH also agrees with Lankhar et al.'s observations from patients with chronic thromboembolic pulmonary hypertension, although the observed increase in peak pressure for the two conditions is much greater than our predictions. However, when we simultaneously increase both the small and large vessel stiffnesses, the observations are then in-line with those of Lankhaar et al. While pressure profiles are modulated by disease, predicted flows in the MPA show negligible effects under disease conditions, unlike results reported by Lankhaar et al., where a significant retrograde flow is observed at the end of systole. This is because the flow profile obtained by MRI measurements from a healthy young subject is imposed even for simulations set up to predict the effect of disease. This is done since no measurements were available for the disease conditions. Maintaining a healthy flow at the system inlet forces the flow to be normal, especially in the proximal locations such as the MPA.

The maximum change in pressure is observed under HLD where pressure increases rapidly with increasing rarefaction of the vascular beds. The pulmonary circulation is normally characterised by negative or open-end type wave reflections (Hollander et al. 2001) which reduce the right ventricular afterload. In the case of HLD, however, the observed increase in a rather featureless pressure waveform suggests that within rarefied vascular beds positive or closed-end reflections develop, amplifying the incident pressure waves and thereby increasing the right ventricular afterload. This hypothesis needs more investigation, but it does indicate that smaller vessels are the site of disease pathophysiology and play important role in improving or worsening the disease condition. HLD significantly raises the mean pressure in the vascular beds, especially in the arteries, enhancing the risk of further small-vessel pathology.

5 Future developments

In the discussion section, we have already highlighted one of the study limitations of imposing a healthy flow profile as inflow boundary condition for simulating the disease condition that prevents the flow to vary in pulmonary hypertension simulations. This aspect should be addressed in future studies predicting dynamics under pathological conditions. In addition, flow in the smallest arterioles and venules (specifically vessels with a radius $<50\,\mu$m), and in the capillaries found around the alveoli, is neglected; this is clearly a topic that merits further investigation and refinement. Absent from our model too is a detailed boundary condition describing the return flow of blood to the left atrium. The contraction of the left atrium causes a biphasic flow profile in the large pulmonary veins, which may propagate upstream. Improvement of this boundary condition could also improve our ability to investigate effects of pulmonary *venous* hypertension, which is associated with left heart condition that may develop due to mitral valve stenosis or congestive heart failure. There is also a need to link this model with a right ventricle model, as remodelling of the heart in disease is clearly linked to disease within the pulmonary circulation. Moreover, the model developed here is only partially patient-specific; we included geometric and flow measurements for the pulmonary arteries, while data from the venous networks were estimated from literature. The haemodynamics, especially the flow distribution, is dependent on vascular dimensions and, with more complete data from a single subject, it will be possible to obtain more detailed patient-specific results. Should future experiments indicate significantly different values of the compliance between the pulmonary arteries and veins, one could also adjust the compliance modulus, which here is assumed constant and the same for the arterial and the venous

trees. This can easily be incorporated by assigning different values to Eh/r_0 in (4) for the arteries and veins.

6 Conclusions

This mathematical and computational model of the pulmonary circulation employs an elegant algorithm that, via calculation of vessel admittance, can be used for merging dynamic predictions in networks containing both arterial and venous trees, a topic rarely studied in the past. The results for the normal physiological case are in agreement with reported pressure range and shape features observed under clinical conditions, and the model provides an important new tool for investigating hypotheses associated with pulmonary hypertension. Despite fixed inflow and boundary conditions, the current simulations set up to predict pressure dynamics associated with PAH, HLD and CTEPH display pressure increases and patterns which are in qualitative (changes in the wave shape and effects on propagation) agreement with results reported in literature.

In conclusion, this is a promising model that can be developed further so that it can be applied to a wide range of pulmonary diseases and used to understand the underlying mechanisms of disease processes.

Acknowledgments Olufsen was funded in part by the National Science Foundation, Award No. NSF-DMS-1122424 and by the National Institute of Health Virtual Physiological Rat Center under Award No. 5-P50-GM094503-02. Vaughan was funded by a studentship from the UK EPSRC. Qureshi was funded by a scholarship from IIU and HEC Pakistan and by PG mobility scholarship from the College of Science and Engineering, University of Glasgow, to visit Olufsen's group.

References

Alastruey J, Parker KH, Peiro J, Byrd SM, Sherwin SJ (2007) Modelling the circle of Willis to assess the effects of anatomical variations and occlusions on cerebral flows. J Biomech 40:1794–1805

Alastruey J, (2011) Numerical assessment of time-domain methods for estimation of local arterial pulse wave speed. J Biomech 44:885–891

Attinger EO (1963) Pressure transmission in pulmonary arteries related to frequency and geometry. Circ Res 12(6):623–641

Azer K, Peskin CS (2007) A one-dimensional model of blood flow in arteries with friction and convection based on the womersley velocity profile. Cardiovasc Eng 7(2):51–73

Barnes PJ, Liu SF (1995) Regulation of pulmonary vascular tone. Pharmacol Rev 47:87–131

Barst RJ, McGoon M, Torbicki A, Sitbon O, Krowka MJ, Olschewski H, Gaine S (2004) Diagnosis and differential assessment of pulmonary arterial hypertension. J Am Coll Cardiol 43:40S–47S

Bovendeerd PH, Borsje P, Arts T, van de Vosse FN (2006) Dependence of intramyocardial pressure and coronary flow on ventricular loading and contractility: a model study. Ann Biomed Eng 34:1833–1845

Burton AC (1972) Physiology and biophysics of the circulation. Year Book Medical Publishers, Chicago, IL, pp 86–94

Castelain V, Herve P, Lecarpentier Y, Duroux P, Simonneau G, Chemla D (2001) Pulmonary artery pulse pressure and wave reflection in chronic pulmonary thromboembolism and primary pulmonary hypertension. J Am Coll Cardiol 7:1085–1092

Clipp RB, Steele BN (2009) Impedance boundary conditions for the pulmonary vasculature including the effects of geometry, compliance, and respiration. IEEE Trans Biomed Eng 56:862–870

Clipp RB, Steele BN (2012) An evaluation of dynamic outlet boundary conditions in a 1D fluid dynamics model. Math Biosci Eng 9:61–74

Cousins W, Gremaud PA (2012) Boundary conditions for hemodynamics: The structured tree revisited. J Comp Phys 231:6086–6096

Cousins W, Gremaud PA, Tartakovsky DM (2013) A new physiological boundary condition for hemodynamics. SIAM J Appl Math 3(73):1203–1233

Dartevelle P, Fadell E, Mussot S, Chapelier A, Hervel P, de Perrot M, Cerrinal J, Laduriel FL, Lehouerou D, Humbert M, Sitbon O, Simonneau G (2004) Chronic thromboembolic pulmonary hypertension. Eur Respir J 23:637–648

Evans RL, Pelley JW, Quenemoen L (1960) Some simple geometric and mechanical characteristics of mammalian blood vessels. Am J Physiol 199:1150–1152

Figueroa CA, Vignon-Clementel IE, Jansen KE, Hughes T, Taylor CA (2006) A coupled momentum method for modeling blood flow in three-dimensional deformable arteries. Comput Methods Appl Mech Eng 195:5685–5706

Fonseca GH, Souza R, Salemi VM, Jardim CV, Gualandro SF (2012) Pulmonary hypertension diagnosed by right heart catheterization in sickle cell disease. Eur Respir J 39(1):112–8

Formaggia L, Lamponi D, Tuveri M, Veneziani A (2006) Numerical modelling of 1D networks coupled with a lumped parameters description of the heart. Comput Methods Biomech Biomed Eng 9:273–288

Fullana J, Zaleski S (2009) A branched one-dimensional model of vessel networks. J Fluid Mech 621:183–204

Fung YC (1996) Biomechanics: circulation, 2nd edn. Springer, New York

Gao Y, Raj UJ (2005) Role of veins in regulation of pulmonary circulation. Am J Physiol Lung Cell Mol Physiol 288:L213–L226

Greenfield JC, Douglas MG (1963) Relation between pressure and diameter in main pulmonary artery of man. J Appl Physiol 18:557–559

Hachulla E, Gressin V, Guillevin L et al (2005) Early detection of pulmonary arterial hypertension in systemic sclerosis: a French nationwide prospective multicenter study. Arthritis Rheum 52:3792–3800

Hall JE (2011) Guyton and Hall textbook of medical physiology, 12th edn. Saunders Elsevier, Philadelphia

Herve P, Musset D, Simonneau G, Wagner W Jr, Duroux P (1989) Almitrine decreases the distensibility of the large pulmonary arteries in man. Chest 96:572–577

Hollander EH, Wang JJ, Dobson GM, Parker KH, Tyberg JV (2001) Negative wave reflections in pulmonary arteries. Am J Physiol Heart Circ Physiol 281:H895–902

Huang W, Yen RT, McLaurine M, Bledsoe G (1996) Morphometry of the human pulmonary vasculature. J Appl Physiol 81:2123–2133

Huo Y, Kassab GS (2007) A hybrid one-dimensional/Womersley model of pulsatile blood flow in the entire coronary arterial tree. Am J Physiol Heart Circ Physiol 292:H2623–H2633

Kato R, Lickfett L, Meininger G, Dickfeld T, Wu R, Juang G, Angkeow P, LaCorte J, Bluemke D, Berger R, Halperin HR, Calkins H (2003) Pulmonary vein anatomy in patients undergoing catheter ablation of atrial fibrillation. Lessons learned by use of magnetic resonance imaging. Circulation 107:2004–2010

Kawahira Y, Kishimoto H, Kawata H, Ikawa S, Ueda H, Nakajima T, Kayatani F, Inamura N, Nakada T (1997) Diameters of the pulmonary arteries and veins as an indicator of bilateral and unilateral pulmonary blood flow in patients with congenital heart disease. J Card Surg 12:253–260

Kim YH, Marom EM, Herndon JE, McAdams HP (2005) Pulmonary vein diameter, cross-sectional area, and shape: CT analysis. Radiology 235:43–50

Krenz GS, Dawson CA (2003) Flow and pressure distributions in vascular networks consisting of distensible vessels. Am J Physiol 284:H2192–H2203

Lankhaar JW, Westerhof N, Faes TJC, Marques KMJ, Marcus JT, Postmus PE, Vonk-Noordegraaf A (2006) Quantification of right ventricular afterload in patients with and without pulmonary hypertension. Am J Physiol Heart Circ Physiol 291:H1731–H1737

Levy BI, Ambrosio G, Pries AR, Struijker-Boudier HA (2001) Microcirculation in hypertension: a new target for treatment? Circulation 104(6):735–740

Li CW, Cheng HD (1993) A nonlinear fluid model for pulmonary blood circulation. J Biomech 26:653–664

Machado RF, Gladwin MT (2010) Pulmonary hypertension in hemolytic disorders: pulmonary vascular disease: the global perspective. Chest 137:30S–38S

Matthys KS, Alastruey J, Peiro J, Khir AW, Segers P, Verdonck PR, Parker KH, Sherwin SJ (2007) Pulse wave propagation in a model human arterial network: assessment of 1-D numerical simulations against in vitro measurements. J Biomech 40:3476–3486

Milnor WR (1989) Hemodynamics, 2nd edn. Williams and Wilkins, Baltimore

Mukerjee D, George D, St Coleiro B et al (2003) Prevalence and outcome in systemic sclerosis associated pulmonary arterial hypertension: application of a registry approach. Ann Rheum Dis 62:1088–1093

Müller LO, Toro EF (2014) A global multi-scale mathematical model for the human circulation with emphasis on the venous system. Int J Num Methods Bio Med Eng. doi:10.1002/cnm.2622

Nichols WW, O'Rourke MF (1998) MacDonald's blood flow in arteries: theoretical, experimental and clinical principles, 4th edn. Edward Arnold, Philadelphia

Olufsen MS (1998) Modeling the arterial system with reference to an anesthesia simulator. PhD Thesis, Department of Mathematics, Roskilde University, Denmark

Olufsen MS (1999) Structured tree outflow condition for blood flow in larger systemic arteries. Am J Physiol Heart Circ Physiol 276:H257–H268

Olufsen MS, Peskin CS, Kim WY, Pedersen EM, Nadim A (2000) Numerical simulation and experimental validation of blood flow in arteries with structured-tree outflow conditions. Ann Biomed Eng 28:1281–1299

Olufsen MS, Hill NA, Vaughan GDA, Sainsbury C, Johnson M (2012) Rarefaction and blood pressure in systemic and pulmonary arteries. J Fluid Mech 705:280–305

Patel DJ, Schilder DP, Mallos AJ (1960) Mechanical properties and dimensions of major pulmonary arteries. J Appl Physiol 15:92–106

Patel DJ, De Freitas FM, Mallos AJ (1962) Mechanical function of the main pulmonary artery. J Appl Physiol 17:205–208

Peacock AJ, Rubin LJ (2004) Pulmonary circulation: diseases and their treatment, 2nd edn. Hodder Arnold Publication, London

Peacock AJ, Murphy NF, McMurray JJV et al (2007) An epidemiological study of pulmonary arterial hypertension. Eur Respir J 30:104–109

Peskin E (1961) Transient and steady-state analysis of electric networks. Van Nostrand Company, Princeton, NJ, pp 304–378

Pollanen MS (1992) Dimensional optimization at different levels at the arterial hierarchy. J Theor Biol 159:267–270

Pries AR, Secomb TW, Gaehtgens P (1995) Design principles of vascular beds. Circ Res 77:1017–1023

Reeves JT, Linehan JH, Stenmark KR (2005) Distensibility of the normal human lung circulation during exercise. Am J Physiol Lung Cell Mol Physiol 288:L419–L425

Reymond P, Merenda F, Perren F, Rüfenacht D, Stergiopulos N (2009) Validation of a one-dimensional model of the systemic arterial tree. Am J Physiol Heart Circ Physiol 297:H208–H222

Sherwin SJ, Franke V, Perio J, Parker K (2003) One-dimensional modelling of a vascular network in space-time variables. J Eng Math 47:217–250

Simonneau G, Galle N, Rubin LJ, Langleben D, Seeger W, Domenighetti G, Gibbs S, Lebrec D, Speich R, Beghetti M, Rich S, Fishman A (2004) Clinical classification of pulmonary hypertension. J Am Coll Cardiol 43:5–12

Singhal S, Henderson R, Horsfield K, Harding K, Cumming G (1973) Morphometry of the human pulmonary arterial tree. Circ Res 33:190–197

Sitbon O, Lascoux-Combe C, Delfraissy JF et al (2008) Prevalence of HIV-related pulmonary arterial hypertension in the current antiretroviral therapy era. Am J Respir Crit Care Med 177:108–111

Steele BN, Olufsen MS, Taylor CA (2007) Fractal network model for simulating abdominal and lower extremity blood flow during resting and exercise conditions. Comput Methods Biomech Biomed Eng 10:39–51

Suwa N, Niwa T, Fukasawa H, Sasaki Y (1963) Estimation of intravascular blood pressure gradients by mathematical analysis of arterial casts. Tohoku J Exp Med 79:168–198

Taylor CA, Draney MT, Ku JP, Parker D, Steele BN et al (1999) Predictive medicine: computational techniques in therapeutic decision-making. Comput Aided Surg 4:231–247

Thurlbeck WM, Churg AM (1995) Pathology of the lungs, 2nd edn. Thieme Medical Publishers, New York

Tuder RM, Yun JH, Bhunia A, Fijalkowska I (2007) Hypoxia and chronic lung disease. J Mol Med 85:1317–1324

Uylings HBM (1977) Optimization of diameters and bifurcation angles in lung and vascular tree structures. Bull Math Biol 39:509–520

Valdez-Jasso D, Haider MA, Campbell AL, Bia D, Zocalo Y, Armentano RL, Olufsen MS (2009) Modeling viscoelastic wall properties of ovine arteries. In: Proceedings of ASME 2009, summer bioengineering conference SBC2009-205640

Vaughan GDA (2010) Pulse propagation in the pulmonary and systemic arteries. PhD Thesis, Faculty of Information and Mathematical Sciences, University of Glasgow, UK

Vignon-Clementel IE, Figueroa CA, Jansen KE, Taylor CA (2006) Outflow boundary conditions for three-dimensional finite element modeling of blood flow and pressure in arteries. Comput Methods Appl Mech Eng 195:3776–3796

van de Vosse FN, Stergiopulos N (2011) Pulse wave propagation in the arterial tree. Annu Rev Fluid Mech 43:467–499

Weibel ER (2009) What makes a good lung? The morphometric basis of lung function. Swiss Med Wkly 139:375–386

Xiao N, Humphrey JD, Figueroa CA (2013) Multi-scale computational model of three-dimensional hemodynamics within a deformable full-body arterial network. J Comput Phys 244:22–40

Yen RT, Rong Z, Zhang B (1990) Elasticity of pulmonary blood vessels in human lungs. In: Farrell Epstein MA, Ligas JR (eds) Respiratory biomechanics: engineering analysis of structure and function. Springer, New York, pp 109–116

Yen RT, Sobin SS (1988) Elasticity of arterioles and venules in postmortem human lungs. J Appl Physiol 64(2):611–619

Zhuang FY, Fung YC, Yen RT (1983) Analysis of blood flow in cats lung with detailed anatomical and elasticity data. J Appl Physiol 55(4):1341–1348